Stress–Strain Predictions of Semisolid Al-Mg-Mn Alloys During Direct Chill Casting: Effects of Microstructure and Process Variables

NASIM JAMALY, A.B. PHILLION, and J.-M. DREZET

The occurrence of hot tearing during the industrial direct chill (DC) casting process results in significant quality issues and a reduction in productivity. In order to investigate their occurrence, a new semisolid constitutive law (Phillion *et al.*) for AA5182 that takes into account cooling rate, grain size, and porosity has been incorporated within a DC casting finite element process model for round billets. A hot tearing index was calculated from the semisolid strain predictions from the model. This hot tearing index, along with semisolid stress–strain predictions from the model, was used to perform a sensitivity analysis on the relative effects of microstructural features (*e.g.*, grain size, coalescence temperature) as well as process parameters (*e.g.*, casting speed) on hot tearing. It was found that grain refinement plays an important role in the formation of hot cracks. In addition, the combination of slow casting speeds and a low temperature for mechanical coalescence was found to improve hot tearing resistance.

DOI: 10.1007/s11663-013-9902-0
© The Minerals, Metals & Materials Society and ASM International 2013

I. INTRODUCTION

HOT tearing is a phenomenon that occurs during the last stages of solidification in which cracks form in the semisolid regime. It is a serious quality defect that is often present in direct chill (DC) cast aluminum cylindrical billets and rectangular ingots. The occurrence of hot tearing in DC casting is usually attributed to the combination of low semisolid permeability and the occurrence of thermal stresses and strains during the casting process, which deform the material in the semisolid state. Industrial practice has traditionally attempted to solve the problem by a "trial and error" process, *i.e.*, by modifying process variables such as casting speed, bottom block geometry, and cooling water flow rate. Fundamental experimental studies of hot tearing have also shed much light on the nucleation and growth of hot tears (see, for example, the review by Eskin *et al.*[2]). Generally, experiments are carried out on a small scale within the lab. But, these results are difficult to interpret with respect to industrial practice simply because the factors that cause hot tears to occur (*e.g.*, thermal stresses and strains) are highly sensitive to casting geometry and manufacturing conditions. Moreover, performing hot tearing experiments on an industrial scale by adjusting the process parameters is time consuming and expensive. These limitations have necessitated the development of a number of DC casting process simulations based on finite elements (FE) that have examined various aspects of the casting process (*e.g.*,[3–5]) and are able to predict the thermal fields and stress–strain evolution within the cast body (*e.g.*,[6–9]. The effect of changes in casting parameters can thus be investigated by examining the concomitant changes in the predictions of stress, strain, and temperature evolution. One of the main findings from these models has been the relative importance of processing parameters on hot tearing.[3] Casting speed is believed to be the most important parameter that affects the formation of hot tearing defects,[4,6] while pouring temperature and cooling water flow rate are of reduced importance.[4] The physical effect of increased casting speed is both an overall increase in the solidification rate and a proportional increase in the thickness of the mushy zone.[6]

The key factor in assessing hot tearing susceptibility using a DC casting process model is the stress–strain predictions made within the semisolid temperature regime. Modeling the metallic alloy semisolid behavior during DC casting has always been a challenge because of the large variation in viscosity and permeability that exists in the transition from liquid to solid states and the stochastic nature of the solidification process itself. One successful approach, initiated by Drezet and Eggeler,[10] has been to use a modified creep law to describe the semisolid behavior of AA5182. In this work, it was assumed that the liquid cannot carry any load, but instead it is carried entirely by the existing solid network. This constitutive law was refined by Haaften *et al.*[11] by considering the critical term to be $(1 - f_{LGB})$, where f_{LGB} is the fraction of grain boundary covered by the liquid, instead of the fraction solid, f_s. A further refinement, to utilize an internal variable to represent the state of cohesion of the mush, was proposed by Ludwig *et al.*[12] An alternative methodol-

NASIM JAMALY formerly Master's Student, and A.B. PHILLION, Assistant Professor, are with the School of Engineering, The University of British Columbia, Kelowna, BC, V1V 1V7, Canada. Contact e-mail: andre.phillion@ubc.ca J.-M. DREZET, Senior Scientist, is with the Computational Materials Laboratory (LSMX), Ecole Polytechnique Fédérale de Lausanne, Station 12, 1015, Lausanne, Switzerland.

Manuscript submitted February 26, 2013.
Article published online July 9, 2013.

ogy for modeling semisolid deformation has been to extend the range of the so-called modified Ludwik equation up to the temperature corresponding to the fraction solid for mechanical coalescence, T_{coal} (*e.g.*,[8,9,13]), and then to assume a low elastic modulus and high yield stress above this point.

The modified Ludwik equation:

$$\sigma(T,\varepsilon,\dot{\varepsilon}) = K(T)(\varepsilon_p + \varepsilon_{p_0})^{n(T)}(\dot{\varepsilon}_p + \dot{\varepsilon}_{p_0})^{m(T)}, \quad [1]$$

where σ is the stress, K is the strain-hardening coefficient, n (m) is the strain-hardening (strain rate sensitivity) exponent, and $\varepsilon(\dot{\varepsilon})$ is the plastic strain (strain rate, s^{-1}), describes the constitutive behavior of a solid across a wide range of temperatures. The offset constants ε_{p_0} and $\dot{\varepsilon}_{p_0}$ are used to circumvent convergence issues. Although the use of Eq. [1] to model semisolid deformation during DC casting is relatively easy to implement within a finite element-based process model, and has the advantage of minimizing false strain accumulation in the semisolid, its main drawback is that there is no link to microstructural features such as grain size and percentage porosity. These microstructural features may vary from the skin to the core of a cast component, resulting in variable semisolid constitutive behavior during the casting process.

Recently, a new constitutive equation for semisolid AA5182 has been proposed[1] which takes advantage of the benefits of the Ludwik equation formulation within a finite element simulation while also including microstructural features such as average grain size and porosity. With respect to hot tearing, this constitutive law is especially useful since it captures solidification characteristics such as the mechanical coalescence point and the rate at which the casting cools. In this work, the new constitutive equation has been incorporated into a DC casting process model for the Al-Mg-Mn alloy AA5182 in order to examine the sensitivity of the semisolid stress–strain evolution during DC casting to microstructural features. AA5182 alloy is a commonly used aluminum alloy for diverse applications ranging from the automotive industry to beverage containers. This alloy was chosen for study in this work because of its high susceptibility to hot tearing and the availability of a semisolid constitutive law[1] that includes the effects of microstructure. A total strain criterion is used as an index to carry out a relative study of hot tearing susceptibility with respect to microstructural features at different locations within the cast billet and process parameters.

II. DESCRIPTION OF THE MODEL

The thermomechanical process model for the DC casting of round billets utilizes the general purpose finite element (FE) software package ABAQUS in order to compute the evolution of temperature, stress, and strain during the casting process. The boundary conditions account for primary cooling through the mold, air gap formation, and secondary cooling where the water hits the billet and flows along its surface.[14] The bottom of the billet is cooled using a constant heat transfer coefficient of 1000 W m^{-2} K^{-1}. Since the purpose of this model is to approximate semisolid strain accumulation, distortions such as butt curl and swell are not taken into consideration.

A. *Finite Element Modeling*

The computational domain is reduced to an axisymmetric geometry from the round billet as a result of symmetry. The dimensions of the domain are 160 and 800 mm in the radial and axial directions, respectively. This domain is made up of 200 layers, each 4 mm in thickness and consisting of 32 identical elements. The gradual increase of the cast length with time is simulated by the incremental addition of horizontal layers into the calculation domain. The time step for adding each layer is calculated from the casting speed and is consistent with the casting procedure (*i.e.*, mold filling times).

B. *Material Properties*

1. *Thermophysical properties*

The thermal conductivity, specific heat, latent heat, and density of the AA5182 alloy were taken from Reference 15 and shown in Table I. The solidification path of the alloy was taken from Reference 16 with T_{sol} = 523 °C and T_{liq} = 637 °C. The combination of the large solidification window and the fact that the amount of eutectic is insufficient to completely cover the grain boundaries[17] makes the AA5182 alloy highly prone to hot tear formation. To properly simulate the DC casting process, the thermophysical properties need to include the change in behavior occurring during solidification, specifically the variation of Young's modulus and coefficient of thermal expansion which occurs with increasing fraction solid. The fraction solid at which the alloy starts to exhibit solid thermal contraction and develop stress is generally[9] considered to be close to the fraction solid for mechanical coalescence. The corresponding temperature is called T_{coal}. Furthermore, as shown by Campbell,[18] hot tears occurring due to deformation of the solid skeleton at temperatures above mechanical coalescence will most probably be healed by interdendritic liquid flow. The result of this assumption is that the Young's modulus (E) and coefficient of thermal expansion (α), taken from Reference 15 and shown in Table II, are only of significant value below T_{coal}, whereas above it, they are reduced to a small value. Note that ABAQUS uses linear interpolation at the boundary between regions.

2. *Constitutive properties*

The constitutive properties were incorporated into the DC casting process simulation through the use of the ABAQUS user-defined subroutine UHARD. At temperatures below T_{sol}, the modified Ludwik equation developed by Alankar and Wells[19] was chosen to simulate the constitutive behavior of the alloy (Eq. [1]). This equation is well suited to describe the transition

Table 1. Summary of Thermophysical Properties Used in the Process Model[15]

Property	Temperature Range	Value
Thermal Conductivity (W m^{-1} K^{-1})	$T < T_{coal}$	$119.2 + 0.623T$
	$T_{coal} \le T \le T_{liq}$	$594 - 0.484T - 0.00048T^2$
	$T > T_{liq}$	$69 + 0.033T$
Specific Heat (J kg^{-1} K^{-1})	$T < T_{coal}$	$897 + 0.452T$
	$T_{coal} \le T \le T_{liq}$	$-994.8 + 8T - 0.0074T^2$
	$T > T_{liq}$	1097
Latent Heat (kJ kg^{-3})		397.1
Density (kg m^{-3})	N/A	2400

Table 2. Summary of Mechanical Properties Used in the Process Model[15]

Property	$T_{25°C} < T < T_{sol}$	$T_{sol} < T < T_{coal}$	$T_{coal} < T < T_{liq}$
$\alpha(°C^{-1})$	$-0.0235 + 2 \times 10^{-5}T + 4 \times 10^{-8}T^2$	-same-	0
E (GPa)	$-0.162T^2 + 7.52T + 71589$	$100.836 - 0.174T$	0.01 @ $T \ge T_{coal} + 10$

Table 3. Parameters of the Modified Ludwik Equation for the AA 5182 Alloy in the Solid State[19]

Parameter	Temperature Range (°C)	Values
K (MPa)	$25 \le T < 331$	$-0.3409T + 361.83$
	$331 \le T \le 500$	$-1.1015T + 613.59$
n	$25 \le T < 206$	$-0.0003T + 0.170$
	$206 \le T < 361$	$-0.0007T + 0.252$
	$361 \le T \le 500$	0
m	$25 \le T < 183$	0
	$183 \le T < 361$	$0.001T - 0.183$
	$361 \le T \le 500$	$0.0003T + 0.069$

from time-independent plasticity at low temperatures (strain hardening) to time-dependent plasticity (viscoplasticity) at high temperatures, since the rheological parameters $K(T)$, $n(T)$, and $m(T)$ are continuous functions of temperature. The values for these parameters are shown below in Table III.

Within the temperature range $T_{sol} < T < T_{coal}$, the constitutive behavior is modeled according to the model proposed by Phillion *et al.*[1] as shown below:

$$\sigma(f_s, f_p, \bar{d}) = f_s \sigma_s (\varepsilon_p + \varepsilon_0)^{n_{ss}(T)} \quad [2]$$

with

$$\sigma_s = (483.5 - 0.77T)\dot{\varepsilon}_p^{(0.205+0.00006T)} \quad [3]$$

$$h = \bar{d}(1 - f_s)^{\frac{1}{3}} \quad [4]$$

$$n_{ss} = -6.35e^{-4}h^2 + 0.0202h \quad [5]$$

where σ_s is the solid flow stress (MPa), $\bar{d}$ is the grain size, h is the thickness of the liquid channels between grains, and n_{ss} is a strain-hardening parameter related to the grain size of the solid skeleton. The phenomenological expression for n_{ss} was determined based on regression analysis of semisolid tensile deformation experiments and microstructure simulations. This formulation enables a link between the semisolid microstructure and the resulting constitutive behavior. The resulting semisolid stress–strain relationships for AA5182 are presented graphically in Figure 1 at (a) various grain sizes and (b) various fractions of solid. As can be seen, the semisolid strength increases with increasing f_s and yet decreases with increasing $\bar{d}$. The strain hardening that occurs is a characteristic of semisolid deformation as previously observed both experimentally[20] and through simulation.[21] Finally, for temperatures above T_{coal}, a low constant yield strength is specified.

C. *Grain Size*

The constitutive law for the semisolid, described above, includes a contribution based on the average grain size, $\bar{d}$. This term is important since a gradient in grain size has been found to exist in DC cast aluminum alloy billets even though such alloys are heavily grain refined.[22–24] In order to incorporate this effect into the simulation, the local grain size has been linked to the cooling rate through the growth restriction factor and the methodology of Easton *et al.*[25] The main driving force behind the gradient in grain size is taken to be the average cooling rate between T_{coal} and T_{liq}; other factors are ignored. Thus,

$$\bar{d} = a + \frac{b}{Q} \quad [6]$$

$$b = 281 + \frac{381}{\dot{T}^{\frac{1}{2}}} \quad [7]$$

$$a = -22.08\dot{T} + 222.88, \quad [8]$$

where a and b are fitting parameters taken from,[25] Q is the growth restriction factor for AA5182 and has a value of 13.54 based on the alloy's composition (Al-4.5 wt pct Mg- 0.35 wt pct Mn), and $\dot{T}$ is the local average cooling rate between T_{coal} and T_{liq}. Using Eqs. [6] through [8], the

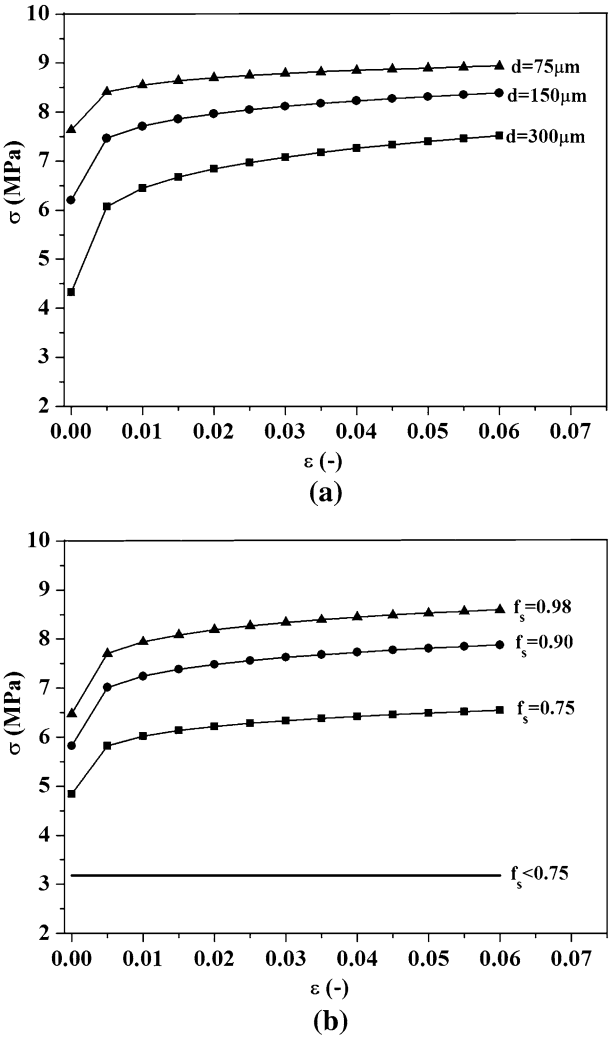

Fig. 1—Semisolid stress–strain response used in the casting simulations for (*a*) $\bar{d} = 300$, 150 and 75 μm at $f_s = 0.98$ and $\dot{\varepsilon} = 10^{-3}$, (*b*) at different f_s for $\bar{d} = 150\mu$m and $\dot{\varepsilon} = 10^{-3}$.

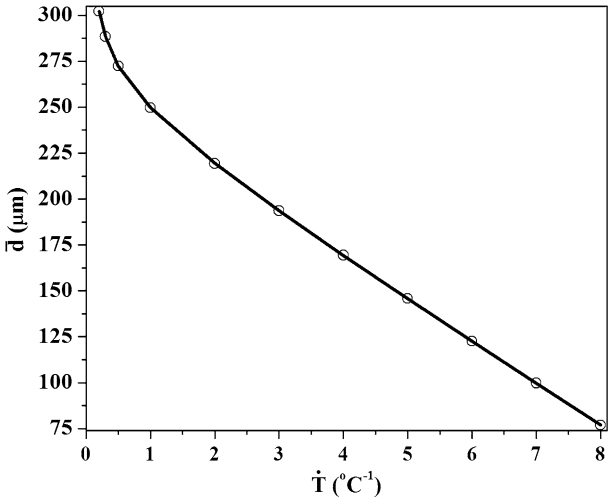

Fig. 2—Effect of cooling rate on grain size ($\bar{d}$) in AA5182, after Easton *et al*[25].

local grain size at each element within the simulation domain can be calculated. The variation of grain size with cooling rate for aluminum alloy AA5182 predicted from Eq. [6] is shown in Figure 2 for the range of cooling rates typically found in DC cast billets.

D. *Hot Tearing Strain*

In order to interpret the simulation results with respect to hot tearing, the term "hot tearing strain" is defined here to be used as a susceptibility index for hot tearing. The concept of this hot tearing strain is inspired by Pellini's total strain criterion,[26] Yamanaka's criterion,[27] and Prokhorov's criterion.[28] The hot tearing strain ε_{HT} is defined as the component of total plastic strain that is perpendicular to the direction of the local thermal gradient. This strain is calculated as follows:

$$\varepsilon_{ij}^{pl} = \begin{bmatrix} \varepsilon_{11} & \varepsilon_{12} \\ \varepsilon_{12} & \varepsilon_{22} \end{bmatrix} \quad [9]$$

$$A = \begin{bmatrix} \cos\theta & \sin\theta \\ -\sin\theta & \cos\theta \end{bmatrix} \quad [10]$$

$$T = A \times \varepsilon_{ij}^{pl} \times A^{t} \quad [11]$$

$$\varepsilon_{HT} = T_{11} + \varepsilon_{33}^{pl}, \quad [12]$$

where ε_{ij}^{pl} are the components of the in-plane plastic strain tensor in the global coordinate system, A is the transformation matrix for a rotation of axis at an angle θ corresponding to the angle between the radial direction and the direction perpendicular to the thermal gradient, T is the plastic strain tensor in the transformed coordinates, and ε_{33}^{pl} is the plastic strain in the out-of-plane or hoop direction. Moreover, the relevant strain for hot tear formation is assumed to be the strain that accumulates only within the brittle temperature region, *i.e.*, T_{coal} to $T(f_s^{0.98})$, where the ductility of the material is at a minimum and thus the semisolid material is most prone to hot tearing. This strain is shown below:

$$\varepsilon_{HT}\text{BTR} = \varepsilon_{HT}(f_s^{0.98}) - \varepsilon_{HT}(f_s^{coal}), \quad [13]$$

where ε_{HT}BTR is the component of plastic strain perpendicular to the thermal gradient that accumulated in the brittle temperature region. If $\varepsilon_{HT}\text{BTR} > 0$, there is a risk of hot tearing because the ductility in the brittle temperature regime is nearly zero.[29] During the last stages of solidification, the dendrites have already bridged and the structure is able to withstand mechanical loading. Thus, hot tears are not likely to occur.

III. RESULTS AND DISCUSSION

The results from the simulations are presented and discussed below. From a processing standpoint, the as-cast microstructure achieved during DC casting of an Al alloy is

Table 4. List of Simulated Processing Conditions

Case	Casting Vel. (mm min^{-1})	T_{coal} (°C)	$\bar{d}$ (μm)	f_s^{coal}
A	66	602	Eq. [6]	0.75
B	66	580	Eq. [6]	0.90
C	40	602	Eq. [6]	0.75
D	66	602	75	0.75
E	66	602	300	0.75

related primarily to the casting speed. This variable will modify the local fraction solid and grain size for a given alloy composition and hence modify the constitutive behavior as outlined in Eqs. [2] through [5]. First, the predictions of stress and strain evolution in the semisolid during DC casting, along with the state of the microstructure, are provided for a given set of conditions. Then, the utility of including microstructural effects within the constitutive law is investigated by comparing the simulations with a variable grain size to simulations where the grain size throughout the domain does not vary. The grain size values used in these cases as input to Eqs. [2] through [5], 75 and 300 μm, are the minimum and maximum values from experimental values measured by Suyitno[22]. Thirdly, the relative effects of casting speed and coalescence temperature on the overall semisolid constitutive response are discussed. The casting velocities are based on industrial values; the mechanical coalescence temperatures, *i.e.*, f_s^{coal}, are taken to represent values of fraction solid, $f_s = 0.75$ and $f_s = 0.90$; and the grain sizes are minimum and maximum values. A list of the various microstructure and process conditions used in the simulations are provided in Table IV. Note that unless otherwise specified, the results refer to the simulation denoted as case *A*.

A. *Stress, Strain, and Thermal Evolution During DC Casting*

The FE simulation provides a detailed description of the evolution of stresses, strains, and temperature during the casting process both in terms of spatial distribution and temporal evolution. In Figure 3, the predicted evolution of (a) hoop stress and temperature and (b) hot tearing strain is provided as a function of time for two different locations within the casting domain for comparison purposes. In (a), the hoop stress is shown since it is considered to be the major driving for hot tear formation. Location X is 60 mm above the bottom block and at the centerline, while Location Y is at the same height, but just below the cast surface. In (b), the ε_{HT} curves only extend to T_{sol} since this measure of strain has no meaning in the solid state. As can be seen from Figure 3(a), point Y cools much faster than point X, owing to the presence of boiling water heat transfer at the surface. Although the hoop stress at point X evolves approximately twice as slowly as point Y, the evolution follows the same trend (*i.e.*, close to zero up to T_{coal}, then through a compression followed by an increasingly tensile regime toward the end of solidification and in the solid state). Turning now to Figure 3(b), it can be seen that there is considerable difference between points X and Y in terms of evolution of ϵ_{HT} with time in the semisolid state. ϵ_{HT} starts to accumulate after the coalescence temperature has been reached. At both X and Y, ϵ_{HT} starts to accumulate in the compressive region, but at the later stages of solidification, only the point at the centerline (X) tends to shift its direction. This behavior implies that the area close to the centerline is more vulnerable to hot tearing.

In Figure 4, two contour plots are provided to show the distribution of $\bar{d}$ and ε_{HT}BTR during casting. The section shown is 600 mm in height and 160 mm in radius. As can be seen in (a), $\bar{d}$ varies from 175 to 275 μm, with the largest grains predicted to form just above the base of the casting. These predictions agree relatively well with the results found experimentally by Suyitno *et al.*[30] for billets that have not been grain refined. The contour plot of ε_{HT}BTR, shown in 4(b) indicates that only a small portion of the billet actually undergoes tensile strain in the brittle region, near the base of the billet and both along the centerline and at the surface. The compressive strains seen further up are a result of the combination of thermal contractions upon cooling and the aggressive surface cooling.

B. *Effect of Microstructure Variations*

Figure 5 shows the variation in hoop stress at a $f_s = 0.98$ along the centerline of the billet and at increasing distance away from the bottom block for the three simulations *A*, *D*, and *E*. In *A*, the variable grain size from Eq. [6] has been used. In *D* and *E*, the grain size is fixed at 75 and 300 μm, respectively. Close to the bottom block, the stress is negative for all cases, and as the distance from the bottom block increases, the hoop stress starts to increase toward the positive side. The stress keeps increasing and reaches a peak value at around 100 mm distance for all the three cases. Beyond this point, the stress starts decreasing again. The stress decreases steadily before reaching a plateau at 400 mm. The distance after which the value of stress remains relatively constant is identified as the start of the steady-state region. From a mechanical point of view, all three simulations (*D* and *E*) reach steady state at a similar point. This is to be expected since the thermal loads (casting speed and cooling rates) are identical.

Figure 6 shows the variation of hot tearing strain along the centerline as a function of the distance from the bottom block for fixed (cases *D* and *E*) and variable (case *A*) grain size simulations. The results predict that there is some variation in the evolution of hot tearing strain due to the variation in grain size, although the

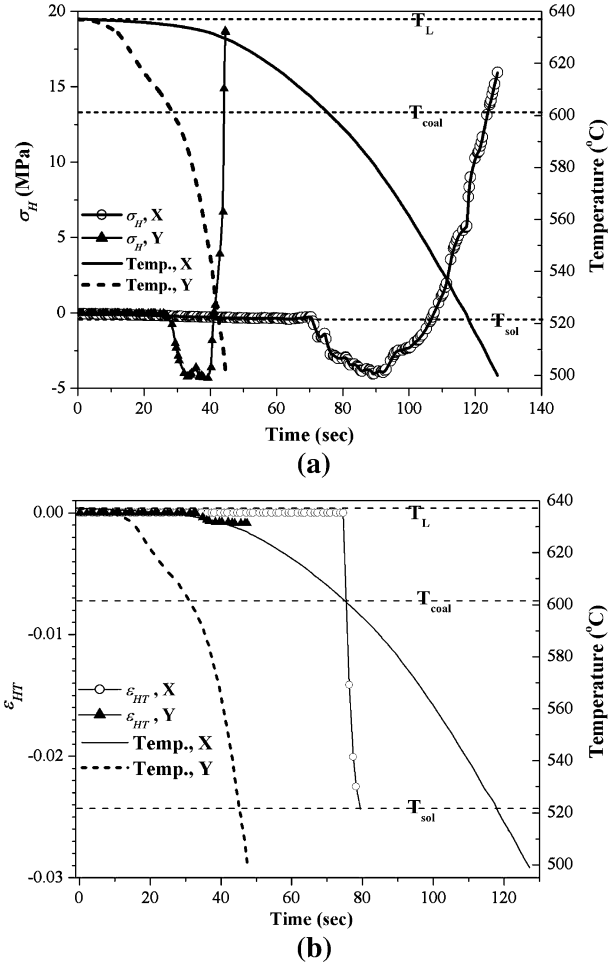

Fig. 3—Evolution in (*a*) σ_H and T with time, and (*b*)ε_{HT} and T with time for case A at locations X and Y; $t = 0$ s corresponds to T_{liq} at each location.

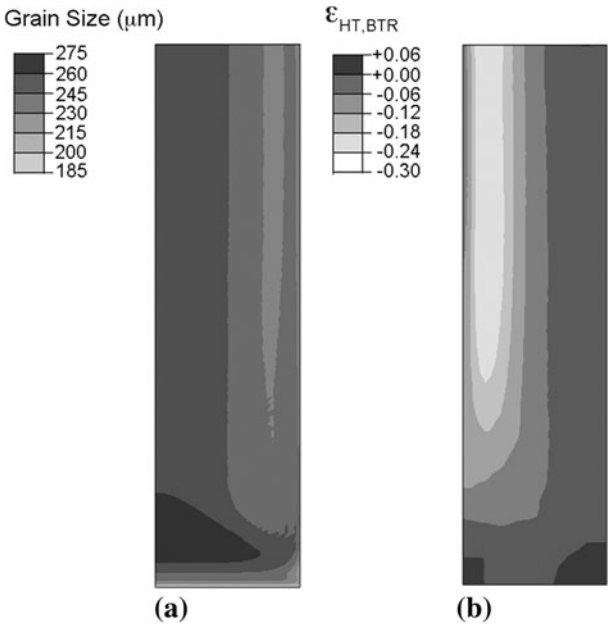

Fig. 4—Contour plots from case A showing (*a*) Grain size and (*b*) Hot tearing strain.

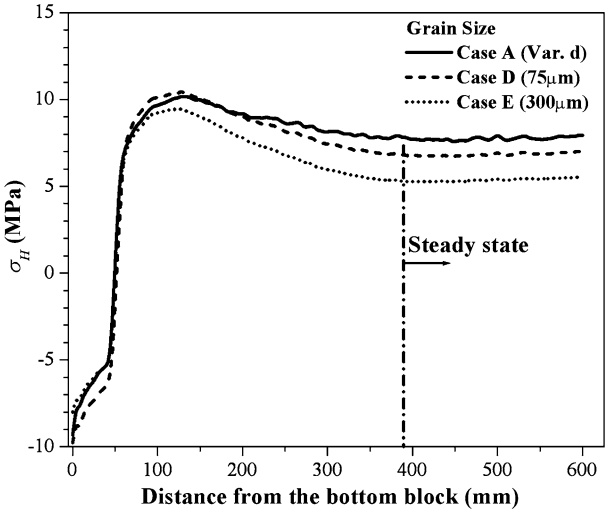

Fig. 5—Variation of σ_H at $f_s = 0.98$ along the centerline of the billet.

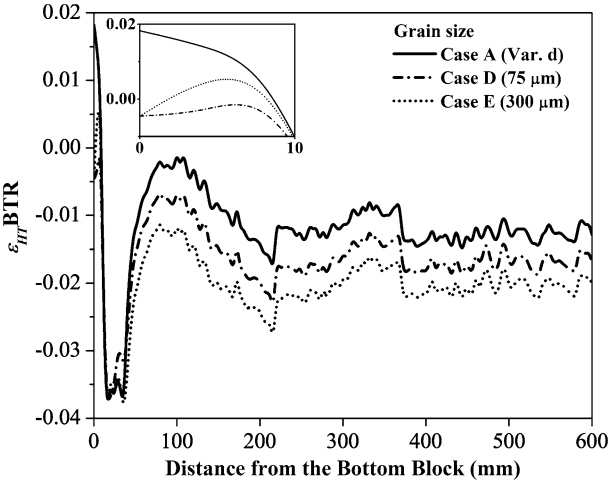

Fig. 6—Variation in ε_{HT}BTR as a function of distance from the bottom block along the centerline. The inset image shows a magnification of the tensile strain near the base of the casting.

trends are similar. The largest strains always occur with the variable grain size simulation, and for the most part the strains are negative except for a small region near the base of the billet. Thus, away from the initial transient, the billet is not susceptible to hot tearing. As can be seen in the inset graph, there is considerable difference in the hot tearing strain in the initial transient. With the variable grain size, in case *A*, the hot tearing strain on the surface (at $z = 0$) is nearly 0.02, whereas the simulations with a fixed grain size have a compressive surface strain. Figure 7 shows the horizontal variation of hot tearing strain as a function of distance from the centerline and 12 mm above the bottom block for the cases *A*, *D*, and *E*.The maximum hot tearing strain is at the center for all three simulations, and is tensile. Hot tearing strains are also tensile near the billet's surface, indicating that both the centerline and surface are prone to hot tearing. As in Figure 6, the highest strains occur

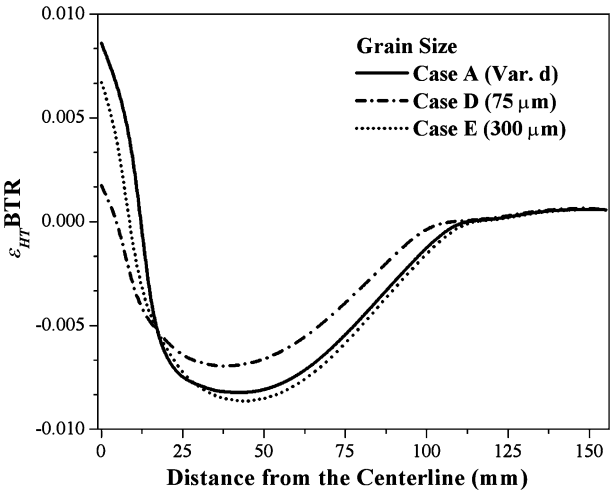

Fig. 7—Variation in ε_{HT}BTR as a function of distance from the centerline at a height of 12 mm above the base of the billet.

in case *A* with variable grain size, while the smallest strains are found in case *D* ($\bar{d} = 75\mu$m).

Overall, this series of simulations indicates that the use of a semisolid strength linked to grain size is important for hot tearing susceptibility. Near the base of the billet, the hot tearing strain is the largest when there is variable grain size because of the resulting variation in the semisolid billet's strength. Regions close to the center, with larger grains as shown in Figure 4, will be weaker than toward the surface and thus will accumulate larger strain. This is due to the fact that the high cooling rate creates small grains near the billet surface, which have a higher yield stress as compared to the large centerline grains and so pass along the strain to the center. It is expected that a semisolid material with large grains, such as the center of the billet, would exhibit higher strain because it possesses lower strength and because the intergranular liquid channels are larger, allowing for more liquid flow. Using the same logic, the structure with the smallest grains, such as case *D*, would acquire the lowest strain, as shown in Figures 6 and 7. Furthermore, case *A* has higher hot tearing strains as compared to case *E* because of the variation in yield strength existing in case *A*. In case *E* ($\bar{d} = 75\mu$m), all of the material has the same semisolid yield strength and so the material closer to the surface cannot pass along the strain to the center. Experimentally, it has been found that although grain refinement generally increases hot tearing resistance, grain refinement below 100 μm actually increases hot tearing tendency in wrought aluminum alloys during casting.[31]

Although the hot tearing strain predictions are not all that different among the three cases *A*, *D*, and *E*, the challenge in this area of research has been to quantitatively predict hot tearing formation in an industrially cast component. As shown in Figures 6 and 7, the inclusion of key details such as semisolid constitutive behavior that is a function of grain size is needed to capture both the macroscale and microscale aspects of this defect. The variation in grain size predicted in the current model leads to a variation in semisolid yield strength at a given temperature and hence to the accumulation of strain in the weakest area, *i.e.*, the large grains contained in the centerline.

C. *Effects of Coalescence Point and Casting Speed*

The simulations denoted *B* and *C* were run in order to determine the effects of mechanical coalescence temperature and casting speed on ε_{HT}BTR. Figures 8 and 9 provide the hot tearing strain in the radial direction at 12 mm above the base of the billet and along the centerline. Beginning with a modification of the coalescence temperature from 602 to 580 °C (case *A* to case *B*), it can be seen that a reduction in coalescence temperature has two contrasting effects on hot tearing strain in the brittle temperature region. First, in the initial transient, ε_{HT}BTR is increased. Second, away from the initial transient, ε_{HT}BTR is significantly compressive. These findings can be compared to experimental work by Eskin and colleagues,[2,32,33] who observed in an AA6061-type alloy that a decrease in T^{coal} decreases hot tearing susceptibility. The decrease in T^{coal} was achieved by grain refinement in a small casting used to measure thermal contraction. In contrast, the effects of grain size and T^{coal} are decoupled in the present study. The present results partially confirm the conclusion of Eskin since, as shown in Figures 6 and 7, smaller grains do result in a reduction in the amount of hot tearing strain obtained during DC casting. However, when T^{coal} is reduced for a given grain size distribution during DC casting, the region of the initial transient may be more susceptible to hot tearing due to the variation in yield strength that exists due to grain size variation. Away from the transient, the grain size is approximately constant, as shown in Figure 4. Since the yield strength will be similar from one semisolid grain to the next, the major effect of a reduction in coalescence temperature is to reduce the processing window for hot tear formation. The grain size variation and complex stress states seen in DC casting are not evident in the previous work.

It can also be seen from Figures 8 and 9 that only a negligible amount of hot tearing strain is accumulated when a slow casting speed of 40 mm/min (case *C*) is used. In fact, the strain along the radial direction and along the centerline is nearly always compressive for this simulation. For a slower casting speed, the material being cast is in contact with the mold and the spray water for longer times. Thus, there is a smaller thermal gradient and hence a smaller differential thermal contraction making this set of processing parameters much more resistant to hot tearing, as observed previously.[13,34] This finding will hold as long as the heat transfer between the water sprays and the billet during secondary cooling remains in the nucleate boiling regime. However, previous research has shown that a lower casting speed also decreases the length of the nucleate boiling zone of secondary cooling[35] and tends to shift the secondary cooling regime from nucleate to film boiling. Consequently, heat transfer is drastically reduced and potentially results in severe hot tear formation.[8]

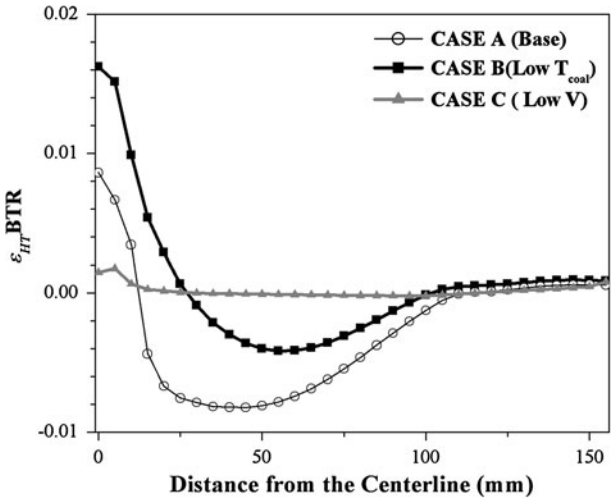

Fig. 8—ε_{HT}BTR as a function of distances from the centerline at a height of 12 mm above the base of the billet for Cases *A*, *B*, and *C*.

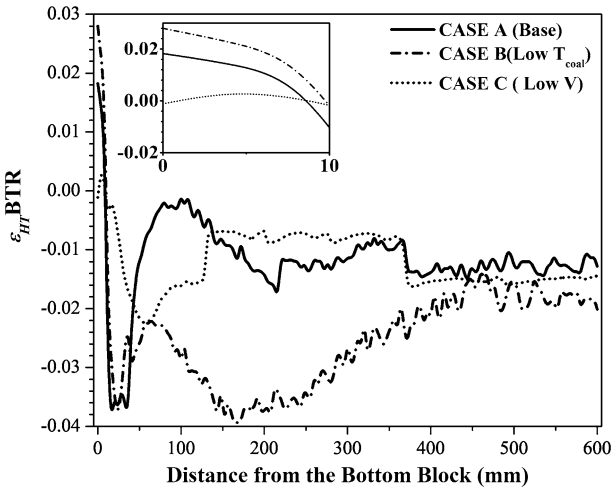

Fig. 9—ε_{HT}BTR at different distances from the bottom block along the centerline for Cases *A*, *B* , and *C*.

The hot tearing strain curves shown in Figures 8 and 9 demonstrate the sensitivity of hot tearing strain within a numerical model on process parameters such as casting velocity and physical parameters such as the T^{coal}. In order to quantitatively predict hot tear formation, such characteristics must also be well documented. Casting velocity, a process parameter, is a known quantity. However, while a number of methods have been developed to determine the temperature when stresses start to be developed and transmitted (*e.g.*,[32]) , *i.e.*, T^{coal}, it is a more complex quantity within a numerical model as it will be a function of many variables including cooling rate and the local alloy composition.

The results as presented are based on process simulations and the constitutive behavior of the AA5182 alloy. However, the findings are applicable for other aluminum alloys that have a long freezing range and thus are susceptible to hot tearing. Grain size control during solidification and a process design that takes into account knowledge of the coalescence temperature will reduce the occurrence of hot tearing in DC casting of aluminum alloys.

IV. CONCLUSIONS

A semisolid constitutive law for the aluminum alloy AA5182 has been incorporated into a thermomechanical simulation of the DC casting process in order to investigate the sensitivity of hot tearing to semisolid microstructure and processing parameters. To facilitate the analysis, a modified index for hot tearing based on strain accumulation in the brittle temperature region has been proposed. The results have shown that microstructure morphology and evolution during solidification should be considered for improving hot tearing predictions in process modeling of Al alloys. Based on an analysis of a series of simulations under different microstructural and processing conditions, the following conclusions can be drawn:

1. The simulations predict that, consistent with industrial observations,[13] the region close to the centerline of the billet and near its base experiences tensile strain in the semisolid and is thus most susceptible to hot tearing.
2. Grain size has a definite effect on semisolid strain accumulation. To a large extent, lowering the grain size reduces the semisolid deformation and thus the possibility of hot tearing.
3. A good understanding of the coalescence temperature is key for predicting hot tearing formation. The assumption of a low coalescence temperature (*i.e.*, at higher fraction solid) increases the vulnerability to hot tearing.

Although the inclusion of microstructure morphology within the constitutive description of the semisolid has been shown to be useful for improving hot tearing predictions, the main limitation of the present work is that it does not take into account macroscale fluid flow. Alloys such as AA5182 are susceptible to macrosegregation during DC casting which will, in turn, modify locally the evolution of fraction solid with temperature, especially in the final stages of solidification. This compositional variation will play a major role in defining the temperature for mechanical coalescence and thus the ability of the mushy zone to resist hot tearing.

ACKNOWLEDGMENTS

The authors would like to thank Dr. Steve Cockcroft from The University of British Columbia for fruitful discussions and acknowledge the financial support of the Natural Sciences and Engineering Research Council of Canada.

REFERENCES

1. A.B. Phillion, S.L. Cockcroft, and P.D. Lee: *Model. Simul. Mater. Sci. Eng.*, 2009, vol. 17, p. 055011.
2. D. Eskin, Suyitno, and L. Katgerman: *Prog. Mater. Sci.*, 2004, vol. 49, pp. 629–711.
3. E. Emley: *Int. Met. Rev.*, 1976, vol. 21, pp. 75–115.
4. H. Nagaumi, K. Aoki, K. Komatsu, and N. Hagisawa: *Alum. Alloys Phys. Mech. Prop. Pts 1–3*, 2000, vol. 331-3, pp. 173–78.
5. A. Williams, T. Croft, and M. Cross: *Metall. Mater. Trans. B*, 2003, vol. 34B, pp. 727–34.
6. M. M'Hamdi, A. Mo, D. Mortensen, and H. Fjaer: in *Light Metals*, TMS, Warrendale, 2002, pp. 695–701.
7. M. Rappaz, J.-M. Drezet, and M. Gremaud: *Metall. Mater. Trans. A*, 1999, vol. 30A, pp. 449–55.
8. J. Sengupta, S. Cockcroft, D. Maijer, and A. Larouche: *Mater. Sci. Eng. A*, 2005, vol. 397, pp. 157–77.
9. J.-M. Drezet and A.B. Phillion: *Metall. Mater. Trans. A*, 2010, vol. 41A, pp. 3396–404.
10. J.-M. Drezet and G. Eggeler: *Scripta Metall. Mater.*, 1994, vol. 31, pp. 757–62.
11. W.V. Haaften, B. Magnin, W. Kool, and L. Katgerman: *Metall. Mater. Trans. A*, 2002, vol. 33A, pp. 1971–80.
12. O. Ludwig, J.-M. Drezet, C. Martin, and M. Suery: *Metall. Mater. Trans. A*, 2005, vol. 36A, pp. 1525–35.
13. H. Hao, D.M. Maijer, M.A. Wells, A.B. Phillion, and S.L. Cockcroft: *Metall. Mater. Trans. A*, 2010, vol. 41A, pp. 2067–77.
14. J.-M. Drezet, A. Burghardt, H.G. Fjaer, and B. Magnin: *Solidif. Gravity*, 2000, vol. 329–3, pp. 493–99.
15. L.F. Mondolfo: *Aluminum Alloys: Structure and Properties.* 1st ed., Butterworths, Waltham, MA, 1976.
16. S. Thompson, S. Cockcroft, and M. Wells: *Mater. Sci. Technol.*, 2004, vol. 20, pp. 497–504.
17. S. Lin, C. Aliravci, and N.I.O. Pekguleryuz: *Metall. Mater. Trans. A*, 2007, vol. 38A, pp. 1056–68.
18. J. Campbell: *Castings.* 2nd ed., Butterworth-Heinemann, Oxford, 1991.
19. A. Alankar and M.A. Wells: *Mater. Sci. Eng. A*, 2010, vol. 527, pp. 7812–20.
20. O. Ludwig, J.-M. Drezet, P. Meneses, C. Martin, and M. Suery: *Mater. Sci. Eng. A*, 2005, vols. 413–414, pp. 14–175.
21. A.B. Phillion, P.D. Lee, and S.L. Cockcroft: *Acta Mater.*, 2008, vol. 56, pp. 4328–38.
22. Suyitno: Ph.D. Dissertation, Delft University of Technology, 2005.
23. M. Erdegren, M.W. Ullah, and T. Carlberg: *Simulation of surface solidification in direct-chill 6xxx aluminum billets.* 3rd Int. Conf. Adv. Solidif. Process., 2012, vol. 27, p. 012013.
24. R. Nadella, D. Eskin, Q. Du, and L. Katgerman: *Prog. Mater Sci.*, 2008, vol. 53, pp. 421–80.
25. M. Easton, D. StJohn, and L. Sweet: *Alum. Cast House Technol. Xi*, 2010, vol. 630, pp. 213–21.
26. W. Pellini: *Foundry*, 1952, vol. 80, pp. 125–37.
27. A. Yamanaka, K. Nakajima, K. Yasumoto, H. Kawashima, and K. Nakai: *Rev. Metall. Cah. D Inform. Tech.*, 1992, vol. 89, pp. 627–33.
28. N.N. Prokhorov: *Russ. Cast. Prod.*, 1962, vol. 2, pp. 172–75.
29. A.B. Phillion, S. Thompson, S. Cockcroft, and M. Wells: *Mater. Sci. Eng. A*, 2008, vol. 497, pp. 388–94.
30. A. Suyitno, D.G. Eskin, V.I. Savran, and L. Katgerman: *Metall. Mater. Trans. A*, 2004, vol. 35A, pp. 3551–61.
31. M. Easton, J. Grandfield, D. StJohn, and B. Rinderer: *Alum. Alloys Pts 1, 2*, 2006, vols. 519–521, pp. 1675–80.
32. D.G. Eskin, Suyitno, J. Mooney, and L. Katgerman: *Metall. Mater. Trans. A*, 2004, vol. 35A, pp. 1325–35.
33. D.G. Eskin and L. Katgerman: *Mater. Sci. Forum*, 2006, vols. 519–521, pp. 1681–86.
34. J.-M. Drezet and M. Rappaz: in *Light Metals*, TMS, Warrendale, 2001, pp. 887–93.
35. D.C. Weckman and P. Niessen: *Metall. Trans. B*, 1982, vol. 13B, pp. 593–602.